SUPPLEMENTARY MATERIALS

Three Dimensional Architecture of Membrane-Embedded MscS in the Closed Conformation

Valeria Vásquez, Marcos Sotomayor, D. Marien Cortes, Benoît Roux, Klaus Schulten, and Eduardo Perozo.

EXPERIMENTAL PROCEDURES

Pegylation. After purification, cysteine mutants at positions S9C, G12C, and Y27C were fully-labeled (10:1, label/monomer) and under-labeled (1:10) with PEG-maleimide [1; 2]. The changes in MscS monomer size were analyzed on SDS-PAGE gels.

Liposome and Spheroplast Patch Clamp. Liposome single-channel currents were obtained in the inside-out configuration under symmetrical (200 mM KCl, 90 mM $MgCl_2$, 10 mM $CaCl_2$, and 5 mM HEPES) conditions, at pH 6. Macroscopic currents were recorded by patch-clamping giant spheroplasts as described elsewhere [3]. Glass pipettes were pulled and fire-polished to resistances between 2 and 2.5 MΩ. Negative pressure on the patch was established by applying suction through a high speed pressure clamp (ALA Scientific Instruments Inc.). Single-channel currents were recorded with a DAGAN 3900 patch-clamp amplifier, and currents were sampled at 10 kHz with an analog filter set to 2 kHz [4; 5].

MD simulations. Two systems were prepared for simulation. The first system contained the recently released structure of MscS at 3.7 Å resolution (residues 27 to 280). The second system contained the EPR-refined model (residues 1 to 178). In both cases the

protein was embedded in a fully hydrated membrane (POPC) environment, as described earlier [6]. Ions were placed randomly to reach concentrations of 200 mM KCl, 90 mM $MgCl_2$, and 10 mM $CaCl_2$ for each system. The resulting systems encompassed 264,000 and 210,000 atoms, respectively.

Simulations were performed using NAMD2.6 [7], the CHARMM27 force-field for lipids and proteins [8], the CMAP correction [9], the TIP3 model for water, and a uniform 1fs time step. Other simulation details were described earlier [6]. Both systems mentioned above were subject to 4ns of equilibration in which lipid tails were melted, water was moved out from the membrane-protein interface, and initial constraints on protein side chains and backbone were stepwise released. Equilibration achieved a good packing of lipids around the protein. For each system six nanoseconds of free dynamics were performed after equilibration.

RESULTS

Biochemical evaluation of MscS cysteine mutants, as determined by size exclusion chromatography and SDS-PAGE gel

We have previously shown [5] that our WT MscS purification conditions are gentle enough to obtain a stable heptameric channel (Figure S1). We evaluated the oligomeric state and stability of all cysteine mutants, following membrane solubilization and purification through SDS-PAGE gels and size exclusion chromatography. The oligomeric properties of the mutants were evaluated from the behavior of purified MscS on gels, which include bands representing the monomer, dimer, and heptamer. Figure S1A shows representative SDS-PAGE gels running cysteine mutants from different regions of MscS. None of the mutants were found to behave (monomer-dimer-heptamer) differently than the WT. Nonetheless, we found that some mutants (especially in the TM3) were more susceptible to SDS, since they had more monomers than higher oligomeric bands.

Hydrodynamic analyses of the cysteine mutants were run in a Superdex 200 HR 10/30 column (Amersham Biosciences, Uppsala, Sweden). All NH_2-terminal and TM1 cysteine mutants showed a similar elution profile as WT MscS. Figure S1B shows two representative mutants Y27C (left panel) and S9C (middle panel). For the TM2 segment we found that some of the mutants (I78C, A79C, and T81C) showed a second peak (Figure S1B). However, the heptamer was at least 2.5 times more abundant than that oligomeric state present in the second peak. The TM3 segment was more vulnerable to cysteine mutagenesis, with 30% of the mutants showing a second peak on the elution

profile (L115C and F127C, left panel of Figure S1B). For these mutants we only collected the heptamer fraction (first peak), which it is as stable as the WT.

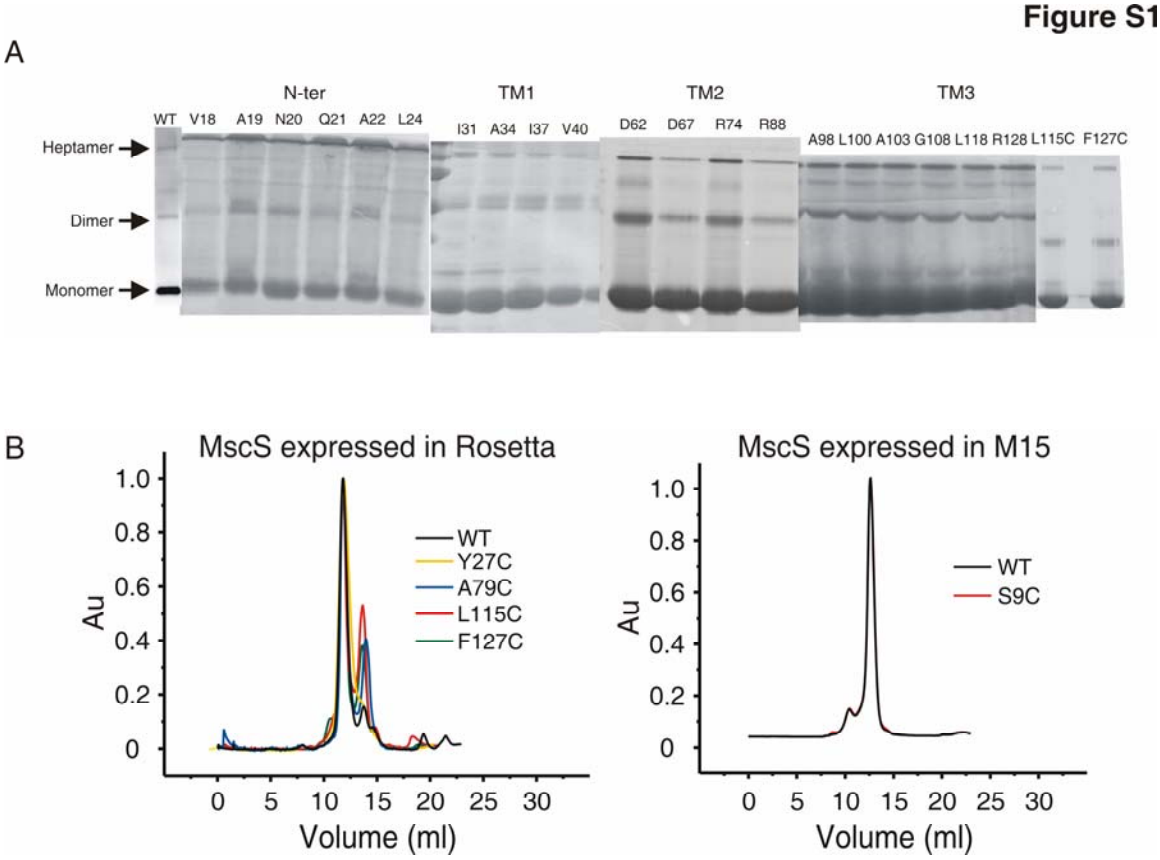

Figure S1. Biochemical evaluation of MscS cysteine mutants. (A) Oligomeric behavior of purified MscS cysteine mutants exhibited in a SDS-PAGE Coomassie-stained gel. The gel shows three possible oligomeric states of the mutants after purification. The cysteine mutants were not treated with DTT or any other reducing agent before running on the gel. (B) Size exclusion chromatography of WT MscS and representative mutants in different *E. coli* strains. Left panel, gel filtration chromatogram of MscS-pET28 WT, Y27C (TM1), A79C (TM2), L115C (TM3), and F127C (TM3) expressed in Rosetta™ cells. Right panel, gel filtration chromatogram of MscS-pQE70 WT and S9C expressed in M15 cells.

Evaluation of MscS closed state in DOPC:POPG reconstituted system, as determined by EPR and by patch clamp techniques

The viability of our model depends on the use and robustness of experimental conditions that stabilize the channel in the closed conformation. We wanted to check that in our lipid system (DOPC:POPG), without changes in lateral tension and voltage, MscS was in the closed state. For this control we took advantage of MscL, another *E. coli* MS channel that its gating has been thoroughly characterized in different lipid systems [10; 11]. We evaluated MscL activation curve in DOPC [11] and DOPC:POPG (Figure S2A). The mid-activation point and the steepness of MscL opening curve was not affected by the composition of this mixed bilayer. Given that the curves were indistinguishable, we can safely predict that in our reconstitution system (black arrow on Figure S2A) MscS should be in the closed state.

Figure S2B shows a representative single-channel trace of MscS in DOPC:POPG, inside-out configuration under patch-clamp conditions, where it is shown that in the absence of negative pressure in the pipette we could not detect any channel activity.

Figure S2

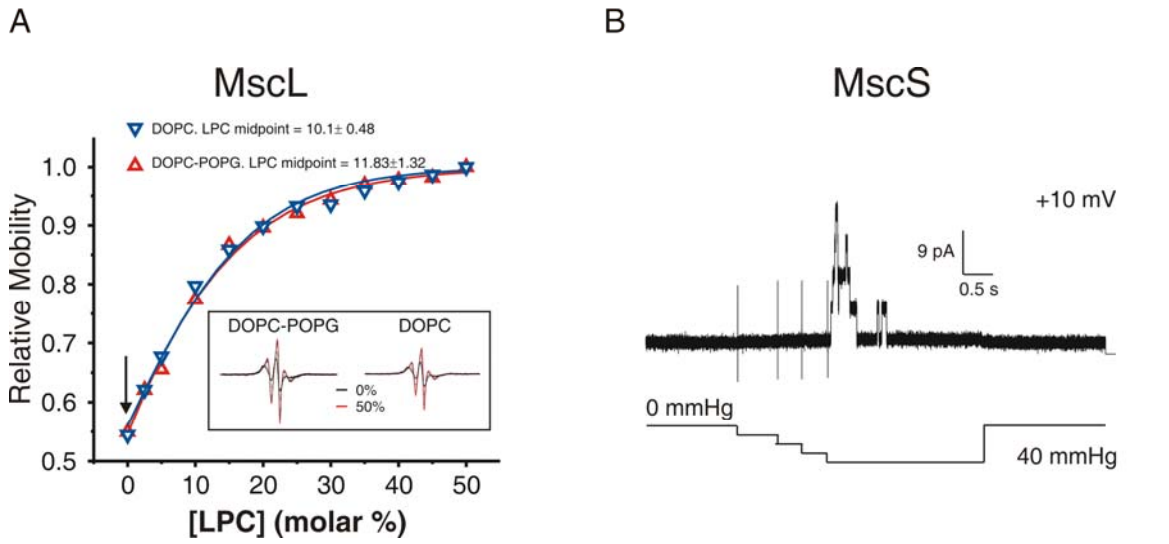

Figure S2. MscS closed state characterization. (A) Concentration dependence of the LPC conformational changes in MscL V23C-SL monitored from the effects on probe dynamics, in DOPC:POPG and DOPC liposomes. The arrow points the condition where MscL is in the closed state. (B) Single-channel record from purified MscS reconstituted in DOPC:POPG lipids. Channel activity was elicited by applying negative transbilayer pressure under patch-clamp conditions.

Labeling efficiency determined by pegylation assay

We did not detect spin-spin coupling in any of the cysteine-labeled positions along the TM domain. Given that we are working with a native, multimeric preparation, one likely interpretation is that the samples under analysis have been under-labeled.

Though Mass Spec would be the technique of choice to determine labeling efficiency, multiple attempts to resolve MscS failed, due to its hydrophobicity. To address this issue, residues with different solvent accessibilities, according to the EPR data (S9C, G12C, and Y27C, Figure S3A), were mass tagged with PEG-maleimide [1; 2] and the changes on MscS size were detected by a gel shift assay (SDS-PAGE gels, Figure S3B). PEG-maleimide is a polyethylene glycol tag that produces a ~ 5 KDa shift upon labeling. Using this approach, it was determined that even under the best conditions (DTT before labeling, and labeling with a 10:1 molar excess of PEG-maleimide) there was still a significant amount of non-reactive monomers(~ 20% for S9C, ~ 10% for G12C, and ~ 40% for Y27C). As expected, this experiment also suggests that the labeling efficiency is highly dependent on the particular position of a cysteine mutant. Therefore we should expect a very low efficiency for mutants on the buried TM3 segment, also the region of the channel that we would expect to find strong spin-spin coupling.

The origin of this under-labeling might be related to the high levels of intrinsic (constitutive) MscS monomers in *E. coli*. We have found, under patch-clamp conditions, (inside-out configuration) an average of 50 channels per patch (~ 1 μm pipette, Figure S3C); this would imply that, qualitatively, each cell might have at least 350 monomers. In any case, it is likely that the MscS population used in the EPR analysis originated from a mixture of WT and cysteine-containing monomers.

Figure S3

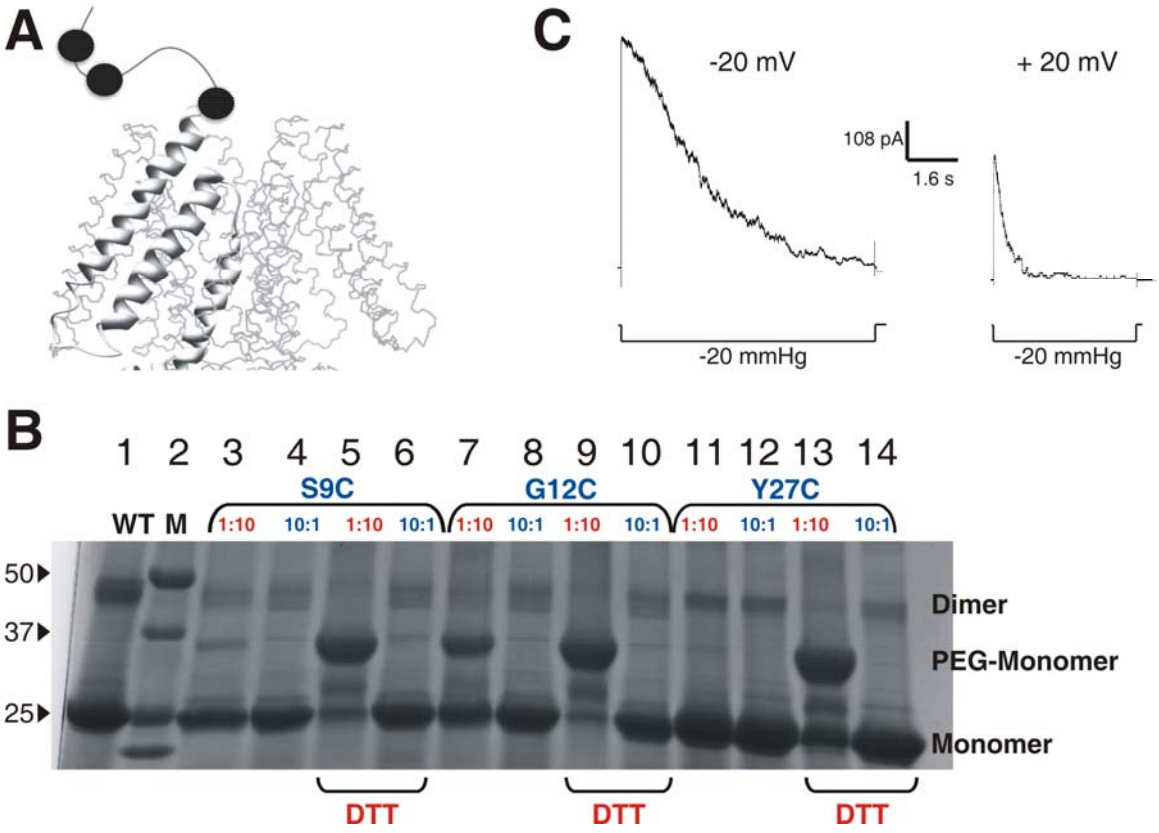

Figure S3. Labeling efficiency as determined by cysteine pegylation [1; 2]. (A) Ribbon diagram showing individual residues with low (S9C) and high accessibilities to NiEdda (G12C and Y27C) as determined by EPR, that were labeled with PEG-maleimide (~ 5 kDa). (B) SDS-PAGE gel stained with Coomassie Blue of mutants labeled with PEG-maleimide. Lane 1: WT MscS, Lane 2: molecular weight marker, Lanes 3-6: S9C, Lane 3: fully-labeled (1 monomer : 10 PEG-maleimides). Lane 4: under-labeled (10 monomers : 1 PEG-maleimide). Lane 5: DTT prior to fully-labeling. Lane 6: DTT prior under-labeling. Lanes 7-10: G12C, Lane 7: fully-labeled. Lane 8: under-labeled. Lane 9: DTT prior to fully-labeling. Lane 10: DTT prior under-labeling. Lanes 11-14: Y27C, Lane 11: fully-labeled. Lane 12: under-labeled. Lane 13: DTT prior to fully-labeling. Lane 14:

DTT prior under-labeling. (C) Macroscopic currents were obtained under constant pressure at +20 mV and -20 mV, at least 66 channels were on the patch.

Vector analysis for Oxygen accessibility parameter

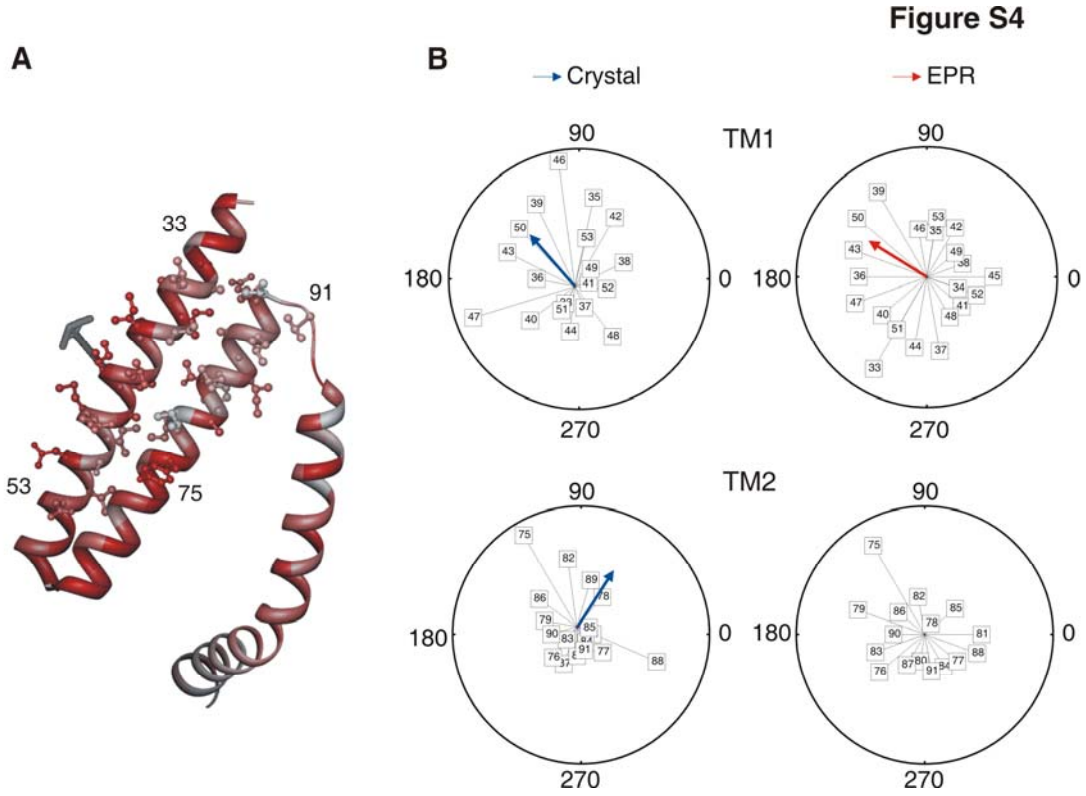

Figure S4. Vector analysis for oxygen accessibility ΠO_2 data. (A) The sum vector for ΠO_2 is plotted in three dimensions on the monomer structure of MscS (gray arrow) pointing in the direction of highest accessibility. Residues used for vector analysis are shown in ball and stick representation. Accessibility to O_2 has been color coded (red-to-white) onto the backbone ribbon of each TM segment. (B) Orientation of the sum vectors for ΠO_2 in TM1 (upper panel) and TM2 (bottom panel) as shown on a helical projection (circle). The blue arrow represents the sum vector for the calculated accessibilities from the crystal structure (2OAU) with the program DSSP [12], and the red arrow represents the sum vector for the experimentally determined O_2 accessibilities.

Residue environmental parameters of the NH_2-terminal segment with His-tag

The initial EPR environmental data of the NH_2-terminus was obtained (Figure S5) from a construct with an NH_2-terminal His-tag that consists of six histidines plus twelve additional residues before the first MscS methionine (pET28a). Even though this segment showed limited periodicity in ΠO_2 and ΠNiEdda, data amplitude had very low contrast. Furthermore, the NiEdda accessibility values were low for a segment that was expected to be at the periplasmic side of the membrane [13]. We expect that these anomalies result from the presence of an NH_2-terminal tag. In order to properly evaluate the structure of the NH_2-terminal segment without the contribution of the His-tag, we used a vector (pQE70) with the His-tag on the COOH-termini, previously shown to be functional and biochemically stable [5].

We evaluated several mutants across the TM segments and compare their mobility spectra. Figure S5B shows a representative comparison of some of the acquired spectra in both constructs for two labeled positions in the TM1, in order to demonstrate that the histidines, either at the N- or C-termini, did not affect the dynamic properties of the TM domain.

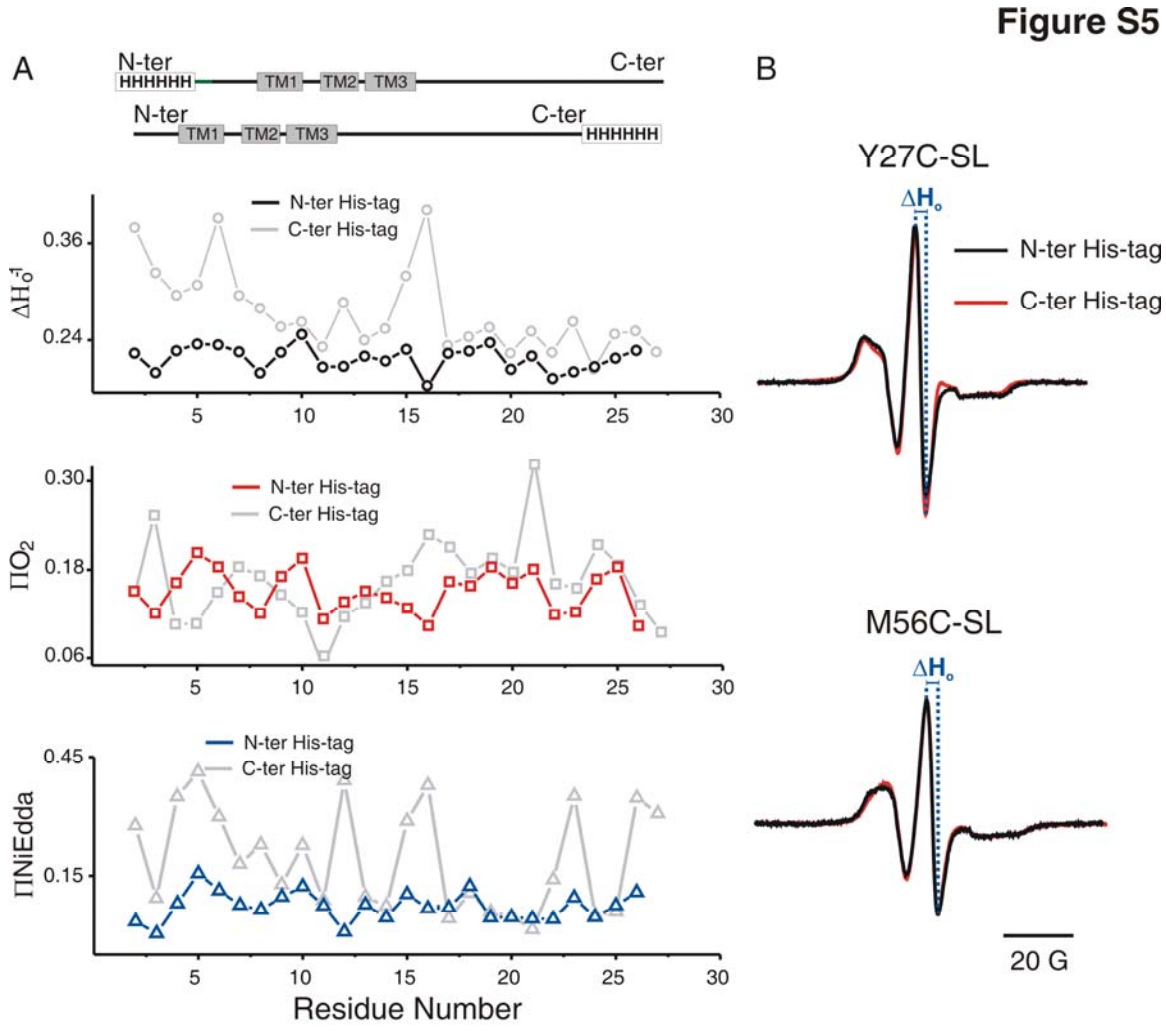

Figure S5. EPR spectroscopy of MscS with an NH_2-terminal His-tag. (A) Residue-specific environmental parameter profiles obtained for the NH_2-terminal segment expressed in pET28 (N-ter His Tag): mobility parameter ΔH_o^{-1} (top, black circles), oxygen accessibility parameter ΠO_2 (middle, red squares), and NiEdda accessibility parameter ΠNiEdda (middle, blue triangles). For comparison purposes, the environmental data obtained for MscS-pQE70, used throughout this manuscript, is plotted in light gray. (B) Comparison of the X-band EPR spectra of two spin-labeled MscS TM1 mutants, purified from the N-terminal His-tag construct (black trace) and

from the C-terminal His-tag construct (red trace), reconstituted in DOPC:POPG liposomes. Also indicated (in blue) is the measurement of the mobility parameter ΔH_o as the peak to peak width of the central line of the spectra.

Fourier transform power spectrum of the NH_2-terminus ΠNiEdda profile

Figure S6

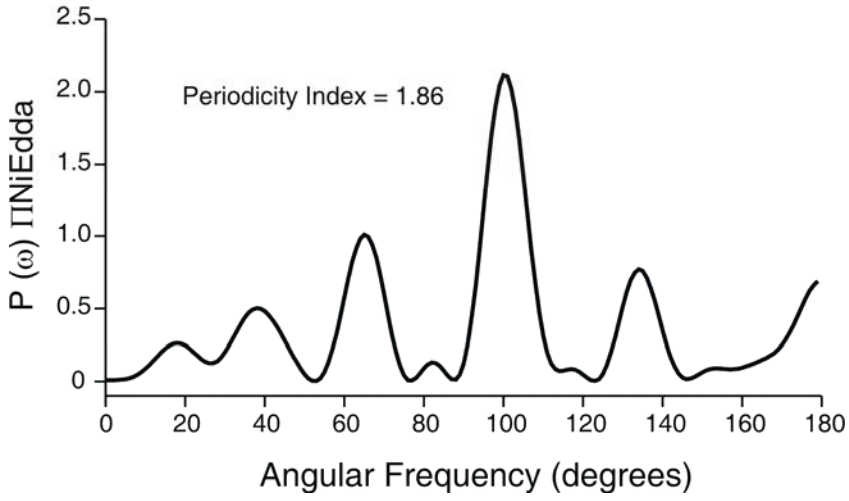

Figure S6. Fourier transform power spectrum of the ΠNiEdda profile. The peak angular frequency is 100^{o}, which corresponds to an α-helical structure.

Environmental phase diagram of MscS' TM domain and NH_2-terminal segment

Figure S7 shows a three-dimensional plot of the environmental parameter data that was used to assign the accessibilities for the EPR-based refinement. This phase diagram takes into account four possible environments: lipidic (O_2), aqueous (NiEdda), proteinaceous (not accessible to O_2 or NiEdda), and interfacial (high O_2 as well as NiEdda accessibility). We have placed the charged residues in this context (circle highlight), to show that most of these positions (when substituted by spin labeled-cysteines) are buried within the protein (R46C-SL, R74C-SL, R74C-SL, and R128C-SL), exposed to NiEdda (R54C-SL and K60C-SL), or with few exceptions exposed to O_2 (R59C-SL and D62C-SL). R59C-SL and D62C-SL, in fact, are in close proximity to residues at the membrane interface, as the DOGS-NTA[Ni(II)]lipids experiments have shown.

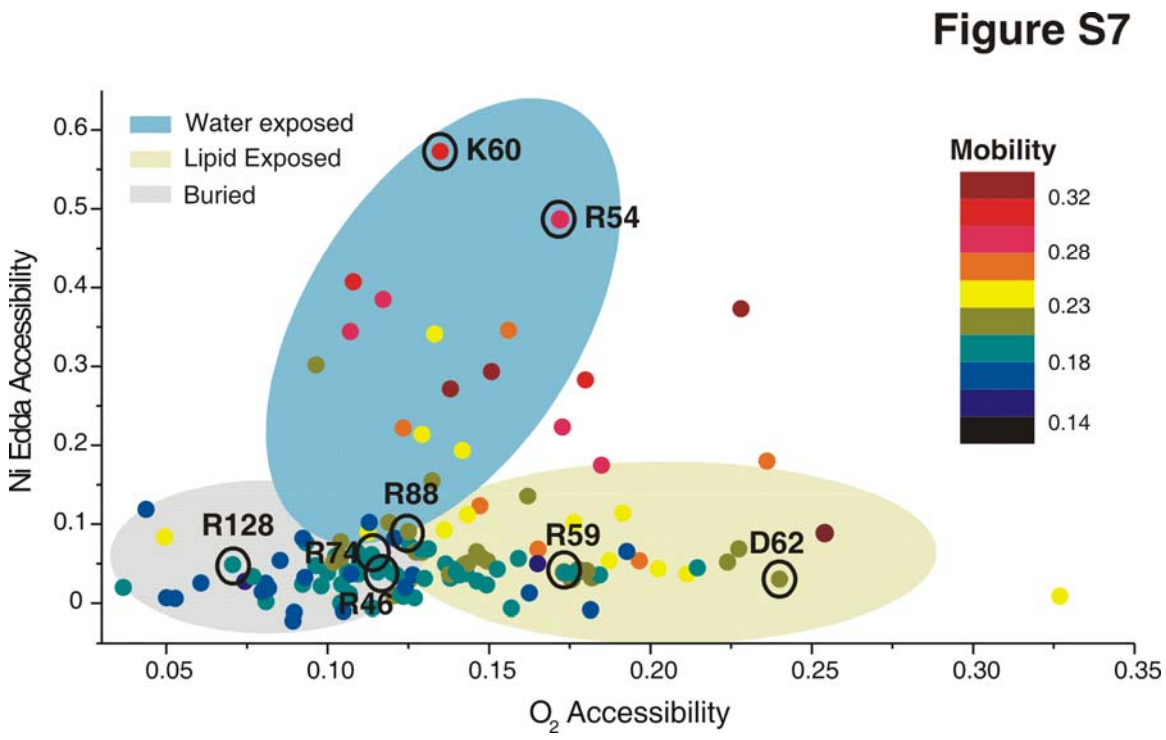

Figure S7. Environmental phase diagram of the NH_2-terminus and TM segments based on mobility parameter ΔH_o^{-1} (scale on the right), oxygen accessibility parameter ΠO_2, and NiEdda accessibility parameter ΠNiEdda. Relevant charged residues are indicated. Only positions with a clearly defined environment were used during refinement.

MD simulations of MscS's crystal structure

The recently released MscS crystal structure (pdb code 2OAU) was simulated for 10 ns as described in Methods. After 4 nanoseconds of equilibration (Figure S8C), release of harmonic constraints to backbone atoms resulted in an asymmetric closure of the transmembrane channel (Figure S8D), as it has been described earlier [6; 14].

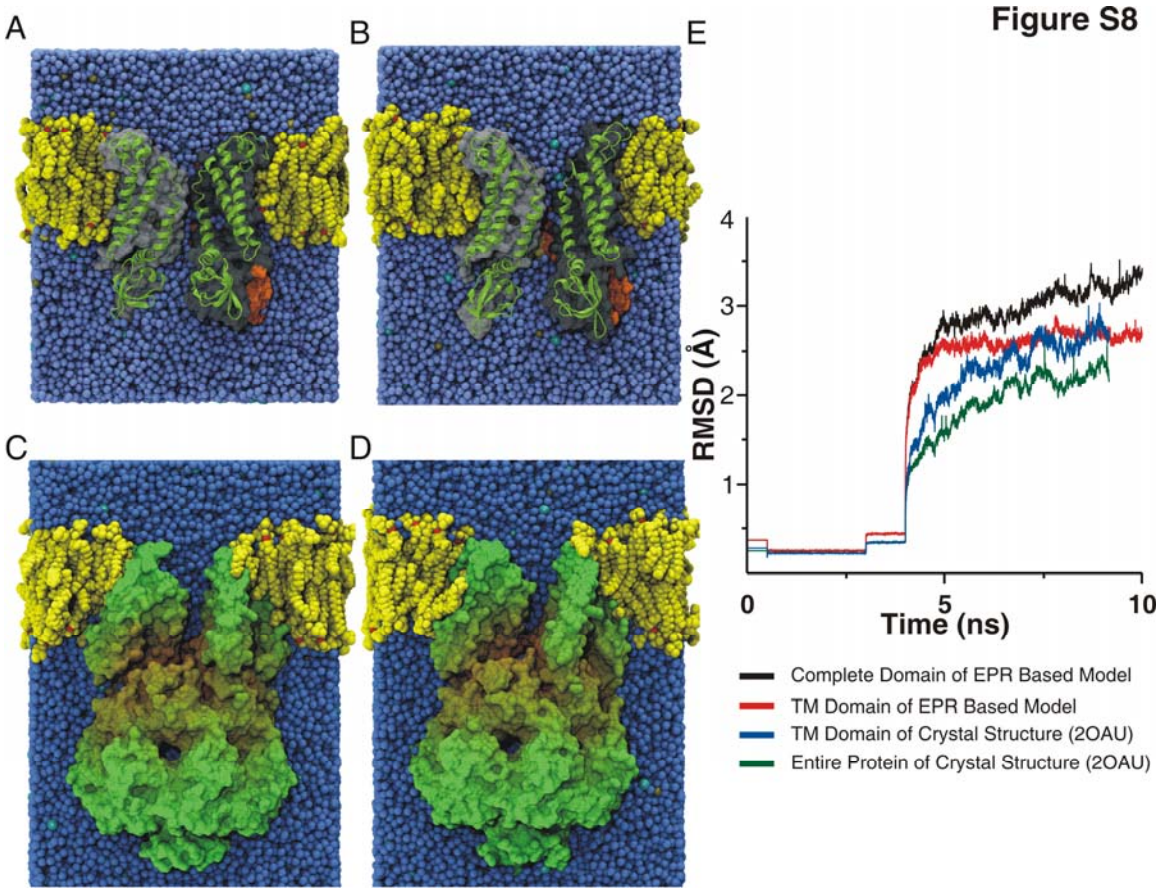

Figure S8. All-atom MD simulations of EPR based MscS model and MscS crystal structure (pdb code 2OAU). (A-B) Snapshots of simulated system after 4 ns of constrained dynamics and 6 ns of free dynamics, respectively. O_2 atoms of water molecules are shown as blue spheres, lipid molecules are shown in yellow, Cl^- ions in cyan, and K^+ ions in ochre. Five out of seven protein subunits are shown in surface representation and colored light gray, dark gray, orange, yellow, and ochre (the latter two

are not visible). Two subunits of the model shown in cartoon representation are superimposed. (C-D) Snapshots of simulated system after 4 ns of constrained dynamics and 6 ns of free dynamics, respectively. O_2 atoms of water molecules are shown as blue spheres, lipid molecules are shown in yellow, Cl^- ion in cyan and K^+ ion in ochre. Five out of seven protein TM subunits are shown in surface representation and colored in green tones according to depth. (E) RMSDs for the complete (black) and TM (red) domain of the EPR based MscS closed model. RMSDs for the complete MscS structure 2OAU are shown for reference (blue, TM domain; green, entire protein). The clearly discernible steps in RMSD arise due to constraints on to the protein relaxed during equilibration.

REFERENCES

1. Lu, J. & Deutsch, C. (2001). Pegylation: a method for assessing topological accessibilities in Kv1.3. *Biochemistry* 40, 13288-301.
2. Lu, J. & Deutsch, C. (2005). Secondary structure formation of a transmembrane segment in Kv channels. *Biochemistry* 44, 8230-43.
3. Martinac, B., Buechner, M., Delcour, A. H., Adler, J. & Kung, C. (1987). Pressure-sensitive ion channel in *Escherichia coli*. *Proc Natl Acad Sci U S A* 84, 2297-301.
4. Sotomayor, M., Vasquez, V., Perozo, E. & Schulten, K. (2007). Ion Conduction through MscS as Determined by Electrophysiology and Simulation. *Biophys J* 92, 886-902.
5. Vasquez, V., Cortes, D. M., Furukawa, H. & Perozo, E. (2007). An Optimized Purification and Reconstitution Method for the MscS Channel: Strategies for Spectroscopical Analysis. *Biochemistry* 46, 6766-6773.
6. Sotomayor, M. & Schulten, K. (2004). Molecular dynamics study of gating in the mechanosensitive channel of small conductance MscS. *Biophys J* 87, 3050-65.
7. Phillips, J. C., Braun, R., Wang, W., Gumbart, J., Tajkhorshid, E., Villa, E., Chipot, C., Skeel, R. D., Kale, L. & Schulten, K. (2005). Scalable molecular dynamics with NAMD. *J Comput Chem* 26, 1781-802.
8. MacKerell, A. D., Bashford, D., Bellot, M., Dunbrack, R. L., Evanseck, J. D., Field, M. J., Fisher, S., Gao, J., Guo, H., Ha, S., Joseph-McCarthy, D., Kunchnir, L., Kuczera, K., Lau, F. T. K., Mattos, C., Michnick, S., Ngo, T., Nguyen, D. T., Prodhom, B., Reiher, W. E., Roux, B., Schlenkrich, M., Smith, J. C., Stote, R.,

Straub, J., Watanabe, M., Wiorkiewics-Kuczera, J., Yin, D. & Karplus, M. (1998). All-Atom Empirical Potential for Molecular Modeling and Dynamics Studies of Proteins. *J. Phys. Chem. B* 102, 3586-3616.

9. Mackerell, A. D., Jr., Feig, M. & Brooks, C. L., 3rd. (2004). Extending the treatment of backbone energetics in protein force fields: limitations of gas-phase quantum mechanics in reproducing protein conformational distributions in molecular dynamics simulations. *J Comput Chem* 25, 1400-15.

10. Perozo, E., Kloda, A., Cortes, D. M. & Martinac, B. (2001). Site-directed spin-labeling analysis of reconstituted Mscl in the closed state. *J Gen Physiol* 118, 193-206.

11. Perozo, E., Cortes, D. M., Sompornpisut, P., Kloda, A. & Martinac, B. (2002). Open channel structure of MscL and the gating mechanism of mechanosensitive channels. *Nature* 418, 942-8.

12. Kabsch, W. & Sander, C. (1983). Dictionary of protein secondary structure: pattern recognition of hydrogen-bonded and geometrical features. *Biopolymers* 22, 2577-637.

13. Miller, S., Bartlett, W., Chandrasekaran, S., Simpson, S., Edwards, M. & Booth, I. R. (2003). Domain organization of the MscS mechanosensitive channel of *Escherichia coli*. *Embo J* 22, 36-46.

14. Spronk, S. A., Elmore, D. E. & Dougherty, D. A. (2006). Voltage-dependent hydration and conduction properties of the hydrophobic pore of the mechanosensitive channel of small conductance. *Biophys J* 90, 3555-69.